Springer

KSME

Journal of Mechanical Science and Technology 31 (10) (2017) 4599~4610
www.springerlink.com/content/1738-494x(Print)/1976-3824(Online)
DOI 10.1007/s12206-017-0906-6

Realizing the empirical mode decomposition by the adaptive stochastic resonance in a new periodical model and its application in bearing fault diagnosis †

Jingling Zhang[1,2], Dawen Huang[1], Jianhua Yang[1,2,3,*], Houguang Liu[1] and Xiaole Liu[1]

[1]*School of Mechatronic Engineering, China University of Mining and Technology, Xuzhou 221116, China*
[2]*Jiangsu Key Laboratory of Mine Mechanical and Electrical Equipment, China University of Mining and Technology, Xuzhou 221116, China*
[3]*Department of Mechanical Engineering, University of Michigan, Ann Arbor, MI 48109, USA*

(Manuscript Received December 9, 2016; Revised June 5, 2017; Accepted June 6, 2017)

Abstract

We investigate a multi-frequency signal that cannot be decomposed by empirical mode decomposition directly. Moreover, this kind of signal in the noisy background cannot be decomposed successfully by the traditional stochastic resonance with bistable system yet. We propose a new method which using the empirical mode decomposition combined the adaptive stochastic resonance in a new periodical model to solve this problem. The results show that the proposed method decomposes the multi-frequency signal perfectly. Meanwhile, the general scale transformation and random particle swarm optimization algorithm are used to help obtain a better result in the process of optimization. Through using this new method, the simulation results are satisfactory. More importantly, this new method also shows good performance in the application of bearing fault diagnosis.

Keywords: Empirical mode decomposition; Adaptive stochastic resonance; Bearing fault diagnosis; Random particle swarm optimization algorithm

1. Introduction

The Empirical mode decomposition (EMD) was put forward by Huang et al. in 1998 to extract the frequencies in a complicated signal [1]. This method decomposes the complicated signal into a series of Intrinsic mode functions (IMF). Through analyzing each IMF, we can receive the features of data information more accurately and effectively. The IMF must satisfy two conditions, one is that the number of the extreme points and the zero-crossing points must be equal or at most one difference in the whole data sequence; the other is that the mean value of the envelope defined by local maximum and local minimum is zero at any points [2]. A complicated signal can be decomposed into the following form by the EMD, *i.e.*,

$$x(t) = \sum_{i=1}^{n} c_i(t) + r_n(t) \tag{1}$$

in Eq. (1), c_i is the ith IMF component and $r_n(t)$ is the residual amount after the IMFS are extracted. Each IMF represents the characteristic frequency of the signal at different time scales and the residual amount represents the information of trend quantity in the original data.

In the field of fault diagnosis, EMD has been applied widely and made some achievements [3-7]. Moreover, the extraction of the characteristic frequency can be achieved an effect by combining the EMD with other methods. Li proposed an improvement EMD method based on the optimized rational Hermite interpolation approach [8]. Yu proposed an application of EMD method and Hilbert spectrum to the fault diagnosis of roller bearings [9]. Liu proposed bearing fault diagnosis method based on hybrid LS-SVM and EMD [10]. Cheng proposed the application of energy operator demodulation approach based on EMD [11]. Cheng proposed a fault diagnosis approach for roller bearings based on EMD method and AR model [12].

In general, some original signal with multi-frequency components can be decomposed successfully by the EMD method. However, the effect of EMD becomes unsatisfactory when the original signal is submerged into the noisy background. The EMD combined with the Stochastic resonance (SR) can be used to deal with this problem [13-17]. The SR is a famous nonlinear phenomenon in which an approximate dose of noise can enhance the weak signal and improve the Signal-to-noise ratio (SNR) of the output [18]. Specifically, the nonlinear system will exhibit SR when SNR reaches its maximum value by optimizing the noise intensity. This kind of SR is called the traditional SR. As the noise intensity increases, the value of SNR will firstly increase and then decrease. The effect of the

*Corresponding author. Tel.: +86 135 1256 7645
E-mail address: jianhuayang@cumt.edu.cn
† Recommended by Associate Editor Byeng Dong Youn

stochastic resonance will come to the best condition until the SNR reaches the maximum value. The signal, noise and nonlinear system achieve the best match at this time. Through the SR processing, the EMD can achieve a better effect than using this method separately.

Although the EMD method is widely applied, some technique problems still exist. One of them, if an original signal cannot be decomposed by EMD directly, whether can it be decomposed successfully with the aid of SR? It is the motivation of this work.

The outline of this paper is arranged as follows. In Sec. 2, we will show an original signal with multi-frequency that cannot be decomposed by EMD successfully. In Sec.3, the method of EMD combined with a general scale transformation adaptive SR will be proposed. Moreover, the adaptive SR will be realized by the random particle swarm optimization algorithm. In Sec. 4, we will present an example where the multi-frequency signal can successfully be decomposed using a combination of SR with a new periodic potential model, whereas decomposition using EMD with the traditional bistable model in failure. The superiority of SR in the periodic model to the SR in the bistable model will be discussed in detail. In Sec. 5, the method of EMD with SR in periodic model will be used to extract the characteristic of the bearing faults. Meanwhile, the method of EMD with SR in bistable system will also be used to make a comparison. The fault frequency and its multiplication will be extracted. Finally, the main conclusions will be drawn in Sec. 6.

2. The multi-frequency signal

Multi-frequency signals are usually encountered in the engineering field. We consider a typical multi-frequency signal. *i.e.*,

$$s(t) = A_1 \cos(2\pi f_1 t) + A_2 \sin(2\pi f_2 t) \tag{2}$$

where $A_1 = 0.1$, $A_2 = 0.2$, $f_1 = 60$, $f_2 = 90$.

We use the traditional EMD method to decompose the signal in Eq. (2) directly. The time domain waveform and the frequency spectrum of the original signal are shown in Figs. 1 and 2, respectively. In Figs. 1 and 2, IMF1 is almost the original signal and the two frequencies cannot be separated into different IMFs. As a result, the signal is decomposed by the EMD method in failure. The reason for the failure is that the parameters of the signal do not satisfy the sufficient condition of successful decomposition [19].

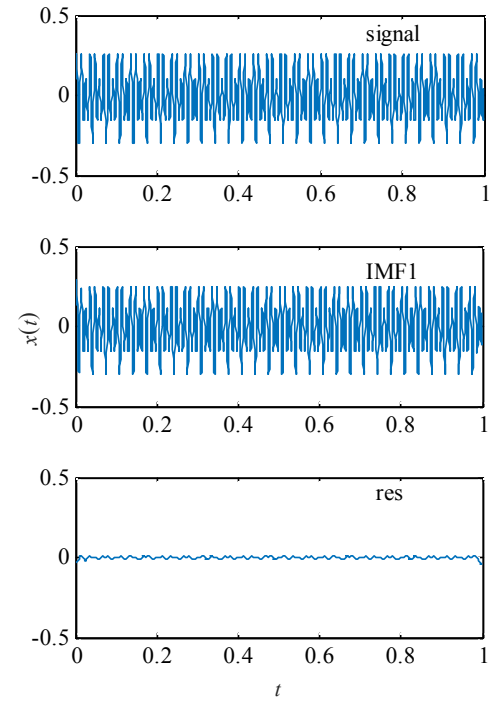

Fig. 1. Time domain waveforms of the original and the decomposed signals.

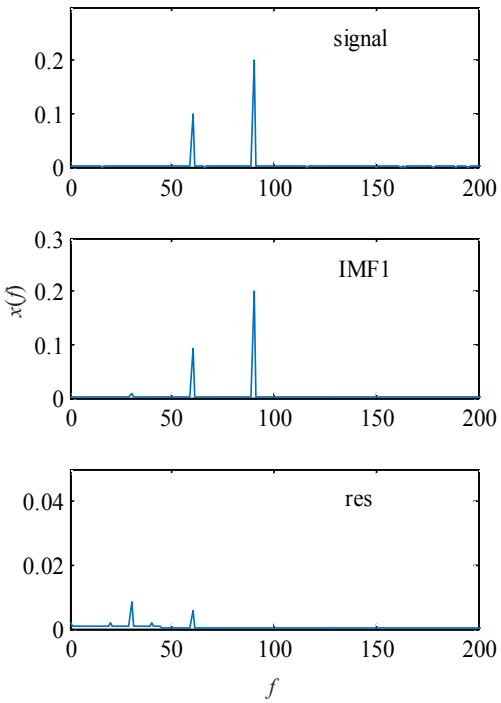

Fig. 2. Frequency spectrums of the original and the decomposed signals.

3. The method of EMD combined with the adaptive SR

In some engineering circumstance, the noise only can be added but not can be reduced. It is a limitation for the application of the traditional SR. To solve this problem, some researchers proposed another kind of SR named adaptive SR in which the excitations are fixed and the system parameters are tuned to induce the SR [20-23]. Usually, the traditional SR occurs under the precondition of adiabatic approximation. In other words, it needs the excitation is weak and the signal is in

low-frequency. However, in the engineering fields, the parameters of the excitations may be in large case. Specifically, the excitation may not be weak and the frequency of the characteristic signal may be ranged from several to thousands Hz. It is another limitation for the application of the traditional SR in engineering field. There are some method can solve this problem, such as the frequency-shifted and rescaling SR [24], the twice sampling SR [25], the multiscale noise tuning SR [26-27]. Among these methods, the multiscale noise tuning SR is an easy and effective method. However, the multiscale noise tuning SR is realized by the normalized scale transformation. Further, through the normalized scale transformation, the output cannot achieve the optimal SR. Hence, in this paper, we will propose a general scale transformation to achieve the optimal SR.

The model of SR is usually governed by the following *Langevin* equation [28-29],

$$\begin{cases} \dfrac{\mathrm{d}x}{\mathrm{d}t} = -U'(x) + s(t) + n(t) \\ \langle n(t) \rangle = 0, \langle n(t), n(0) \rangle = 2D\delta(t) \end{cases} \tag{3}$$

in Eq. (3), $s(t)$ is the weak signal. In this paper, we focus on the multi-frequency signal. Hence, we let

$$\begin{cases} s(t) = \sum_{j=1}^{N} A_j \sin(\omega_j t) \\ \omega_j = 2\pi f_j \,. \end{cases} \tag{4}$$

Here in $n(t)$ is Gaussian white noise. D is the intensity of noise. $\delta(t)$ is the delta function.

In terms of the traditional bistable system, its potential function is

$$U(x) = -\frac{a}{2}x^2 + \frac{b}{4}x^4 \,. \tag{5}$$

In Eq. (5), $a > 0$ and $b > 0$ are the system parameters.

Besides the bistable potential, there are some other potential functions in which the SR can be appearance. Among them, the periodic potential is a new type [30-34]. For example, Nicolis first proposed the SR in multistable system [30], Saikia explored the role of damping on SR in a periodic potential [31], Liu and his co-workers found the SR in periodic potentials driven by colored noise [32]. We also did some works on the dynamics of the system with periodic potential. In Ref. [33], we found that the sequential vibrational resonance distinguishes from the traditional multiple vibrational resonance because its appearance is much more regular and the presence of the resonance is periodic. We also discover adaptive SR with periodic potential has more advantages than adaptive SR in the bistable model [34]. These articles confirm that the periodic potential system is much more superior and worth to apply. The concrete expression of the periodic potential is

$$U(x) = -a\cos(bx) \,. \tag{6}$$

The shapes of bistable potential function and periodic potential function are shown in Fig. 3. Herein, Fig. 3(a) shows the double potential function. The highest point locates at zero which is the unstable state and the lowest points locate at $\pm\sqrt{a/b}$ which are stable states. The height of the barrier is $a^2/(4b)$. In Fig. 3(b), the periodic potential function is described. $\Delta U = 2a$ is the height of potential barrier and the distance between two adjacent high points is $2\pi/b$. The difference between Figs. 3(a) and (b) is that the height changes with the change of width in bistable potential, but the height is independent of the width in the periodic potential system.

Substituting Eq. (5) into Eq. (3), then Eq. (3) can be written as

$$\frac{\mathrm{d}x}{\mathrm{d}t} = ax - bx^3 + s(t) + n(t) \,. \tag{7}$$

Eq. (6) leads to Eq. (3) in the form

$$\frac{\mathrm{d}x}{\mathrm{d}t} = -ab\sin(bx) + s(t) + n(t) \,. \tag{8}$$

Eq. (8) is the model of SR with periodic potential. For simplify, we label the SR in the system with bistable potential and periodic potential as BSR and PSR, respectively.

In order to realize the general scale transformation, some variables are introduced, specifically,

$$x(t) = z(\tau), \tau = mt \,. \tag{9}$$

For bistable system, substituting Eq. (9) into Eq. (7), Eq. (7) can be written as

$$\begin{cases} m\dfrac{\mathrm{d}z}{\mathrm{d}\tau} = az - bz^3 + \sum_{n=1}^{N} A_n \sin\left(2\pi\dfrac{f_n}{m}\tau\right) + n\left(\dfrac{\tau}{m}\right) \\ n\left(\dfrac{\tau}{m}\right) = \sqrt{2Dm}\,\xi(\tau) \end{cases} \tag{10}$$

where m is the scale of time.

Eq. (10) is expressed as

$$\begin{cases} \dfrac{\mathrm{d}z}{\mathrm{d}\tau} = \dfrac{a}{m}z - \dfrac{b}{m}z^3 + \sum_{n=1}^{N}\dfrac{A_n}{m}\sin\left(2\pi\dfrac{f_n}{m}\tau\right) + \sqrt{\dfrac{2D}{m}}\xi(\tau) \\ \langle \xi(\tau) \rangle = 0, \langle \xi(\tau), \xi(0) \rangle = \delta(\tau) \,. \end{cases} \tag{11}$$

Eq. (11) is the equivalent form of Eq. (7). In addition, the system parameters a/m and b/m are unequal in the general scale transformation.

For periodic potential system, substituting Eq. (9) into Eq. (8), Eq. (8) can be written as

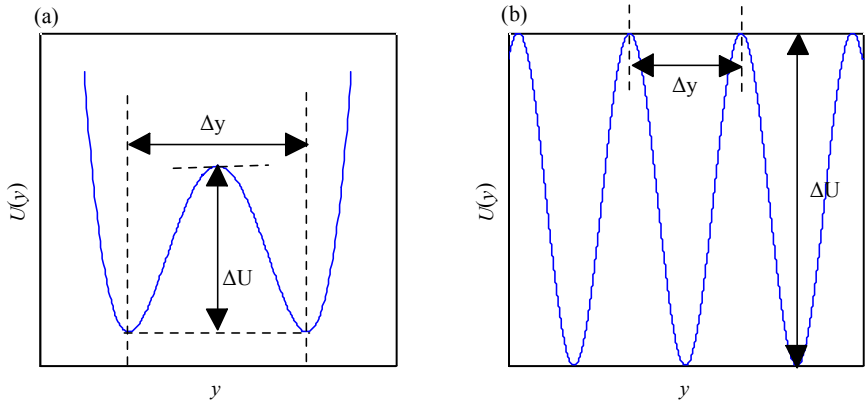

Fig. 3. Shape of the nonlinear potential function: (a) Bistable potential function; (b) periodic potential function.

$$\begin{cases} m\dfrac{\mathrm{d}z}{\mathrm{d}\tau} = -ab\sin(bz) + A\sin\left(2\pi\dfrac{f}{m}\tau\right) + n\left(\dfrac{\tau}{m}\right) \\ n\left(\dfrac{\tau}{m}\right) = \sqrt{2Dm}\xi(\tau)\,. \end{cases} \tag{12}$$

Then this equation can be sorted as

$$\begin{cases} \dfrac{\mathrm{d}z}{\mathrm{d}\tau} = \dfrac{-a}{m}b\sin(bz) + \dfrac{A}{m}\sin\left(2\pi\dfrac{f}{m}\tau\right) + \sqrt{\dfrac{2D}{m}}\xi(\tau) \\ \left\langle\xi(\tau)\right\rangle = 0, \left\langle\xi(\tau),\xi(0)\right\rangle = \delta(\tau) \end{cases} \tag{13}$$

where m is the scale of time and the system parameters a/m and b can be obtained their optimal values by the optimization algorithm. Meanwhile this type of equation can be solved by the fourth-order Runge-Kutta algorithm [35].

To improving the efficiency, different optimization algorithms can be used. In this paper, the random particle swarm optimization algorithm [36-39] is applied to obtain the optimal parameters of the system in the adaptive SR. The SNR is set as the evaluation index in the calculation. SNR is defined as the ratio of signal power to noise power. It is widely used to evaluate whether the system achieves the optimal output [40]. The concrete of the SNR is defined as

$$\begin{cases} SNR = 10\log_{10}\left(\dfrac{S(f)}{N(f)}\right) \\ S(f) = |X(k)|^2 \\ N(f) = \dfrac{1}{2M}\sum_{j=1}^{M}(|X(k-j)|^2 + |X(k+j)|^2)\,. \end{cases} \tag{14}$$

In Eq. (14), f is the frequency of the input signal and k is the serial number of f. $S(f)$ is the power of the input signal and $N(f)$ is the average power of the noise. M is selected according to sampling points N and sampling frequency f_s.

The main steps of the random particle swarm optimization algorithm are as follows:

Step 1: Giving the initialization condition. Setting the learning factors, the mean of the random weight, the number of iterations, the number of particles and the spatial dimension.

Step 2: Initializing individuals of a population. Initializing the position and speed randomly.

Step 3: Calculating the fitness of each particle and finding the local optimal and global optimal.

Step 4: Entering the main loop. Firstly, updating the position and velocity of the particle. Secondly, recalculating the fitness of each particle and updating the local optimal and global optimal. Finally, judging whether the maximum number of iterations has been reached. If not, continuing the loop. If reached, go to the next step.

Step 5: Obtaining the best result.

The specific process of the signal processing based on adaptive SR and EMD is shown in Fig. 4.

4. Numerical simulation

In this section, we verify our method proposed in Sec. 3 by the multi-frequency signal in Sec. 2.

4.1 EMD combined with BSR

In this section, the signal in Eq. (2) is submerged into the Gaussian white noise, specifically

$$x(t) = s(t) + n(t) \tag{15}$$

where $s(t)$ is defined in Sec. 2, $n(t)$ is the Gaussian white noise with intensity D. According to the sampling theory, the sampling frequency should be larger than twice the signal frequency. Whether the sampling point is second power or not, it has little influence on accuracy and speed of the calculation because of the rapid computation of the computer. Since the frequencies are integer in numerical simulation, the high resolution is not necessary. So the simulation parameters are set as f_s = 10000, N = 2000 and then resolution is 10000/2000 = 5. In this subsection, we deal with the signal by EMD combined with BSR. In terms of the EMD by BSR at 60 Hz, D is set as 0.2. Rescaling factor m is set as 600 in general scale transformation, then the fre-

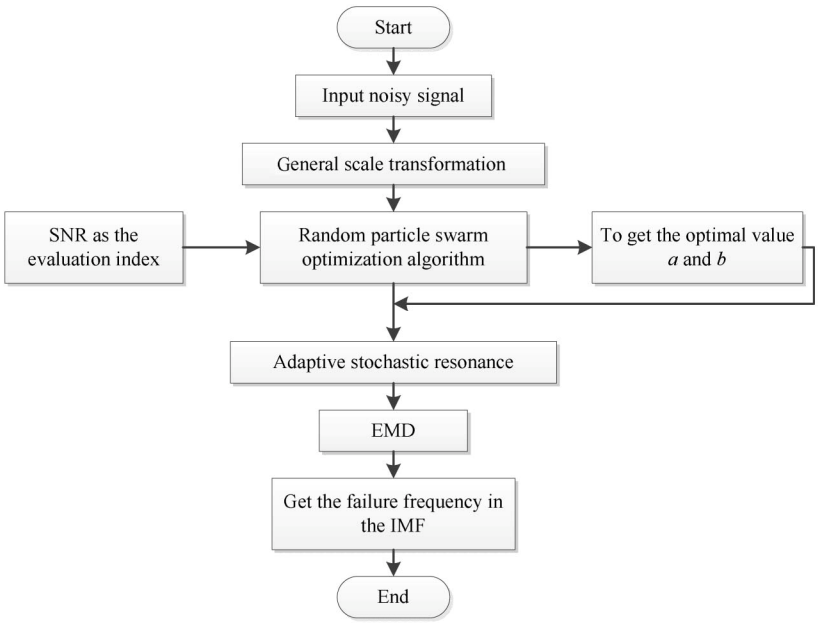

Fig. 4. Flowchart of the signal processing, shows a procedure of adaptive SR and EMD.

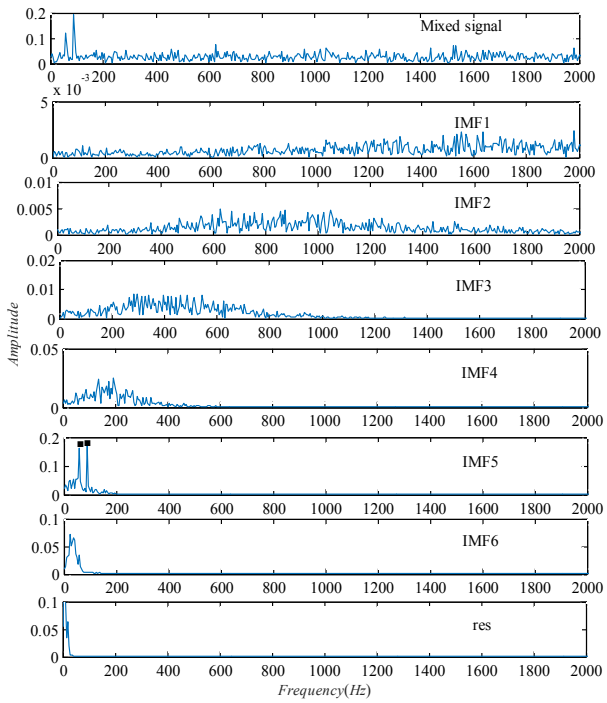

Fig. 5. The frequency spectrum of EMD by BSR at 60 Hz: Optimal output with $a = 0.2442$ and $b = 1021.2$. In IMF5, the first highest point is located at 60 Hz, and the second highest point is located at 90 Hz.

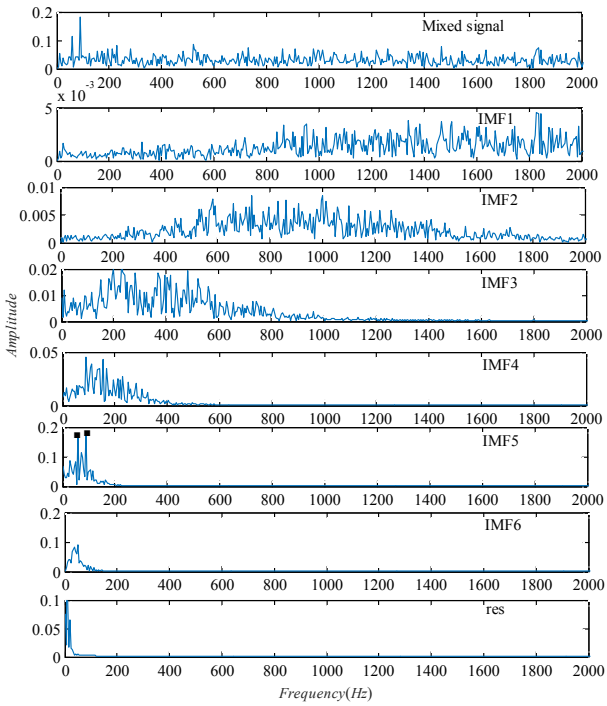

Fig. 6. The frequency spectrum of EMD by BSR at 90 Hz: Optimal output with $a = 1.1179$ and $b = 1322.4$. In IMF5, the first highest point is located at 60 Hz, and the second highest point is located at 90 Hz.

quency rescaled is 60/600 = 0.1<<1 and meets the condition of SR. In fact, the SNR here is the local SNR and $N(f)$ is the noise intensity in the vicinity of signal frequency. So M is set as 10. When dealing with the EMD by BSR at 90 Hz, the parameters are set as $D = 0.3$, $m = 900$, $M = 10$.

Fig. 5 shows the frequency spectrum of the EMD by BSR at 60 Hz. In the frequency spectrum, there are two clear highest points in IMF5. They are located at 60 Hz and 90 Hz, respectively. Due to different frequencies appear in one IMF, it is one kind of mode mixing problems.

Fig. 6 shows the frequency spectrum of the EMD by BSR at 90 Hz. Fig. 6 is similar to Fig. 5 as it also appears the mode

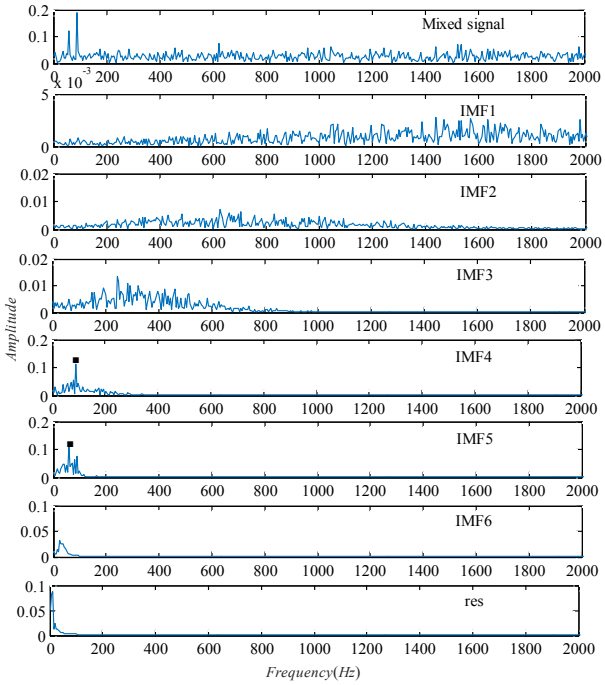

Fig. 7. The frequency spectrum of EMD by PSR at 60 Hz: Optimal output with a = 58.005 and b = 2.1648. In IMF4, the highest point is located at 90 Hz. In IMF5, the highest point is located at 60 Hz.

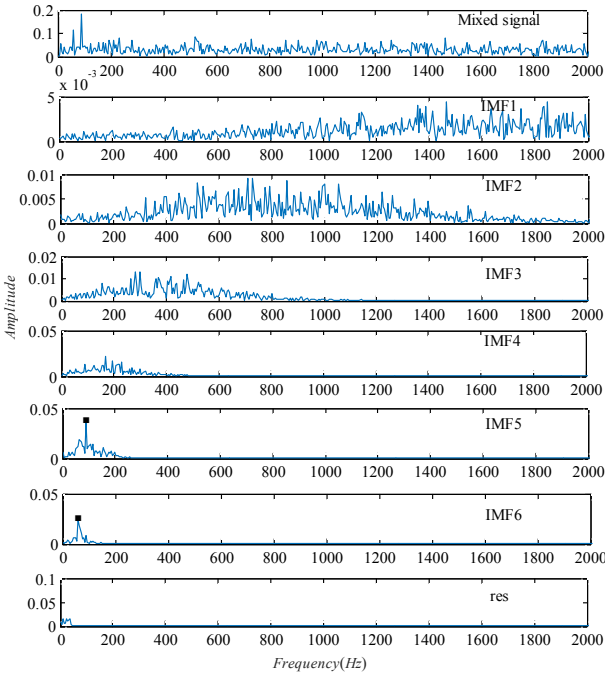

Fig. 8. The frequency spectrum of EMD by PSR at 90 Hz: Optimal output with a = 744.4556 and b = 1.9595. In IMF5, the highest point is located at 90 Hz. In IMF6, the highest point is located at 60 Hz.

mixing problem. Hence, the EMD combined with the traditional BSR is failure in dealing with the multi-frequency signal.

4.2 EMD combined with PSR

In this section, the noisy signal in Eq. (15) is treated by EMD combined with PSR. When dealing with the EMD by PSR at 60 Hz, simulation parameters are set the same as the parameters in the solution of EMD by BSR at 60 Hz. In terms of EMD by PSR at 90 Hz, simulation parameters are set the same as EMD by BSR at 90 Hz.

Fig. 7 shows the frequency spectrum of EMD by PSR at 60 Hz. In the frequency spectrum, the highest points at 60 Hz and 90 Hz appear in IMF4 and IMF5, respectively.

Fig. 8 shows the frequency spectrum of EMD by PSR at 90 Hz. As Fig. 7, it also shows the same phenomenon. Gratifyingly, the multi-frequency is decomposed successfully. It solves the problem appearing in Figs. 5 and 6.

In this section, we obtain that the method of EMD combined with PSR is superiority to the method of EMD combined with BSR in dealing with the multi-frequency signal especially when the signal is submerged into the noisy background.

5. Experimental verification

Rolling bearing fault signals show typical characteristics of nonstationarity, modulation and weakness. The feature information is usually submerged into the noisy background. Hence, it is difficult to extract the weak feature information. In this section, the original data come from the Case Western Reserve University (CWRU) [41] is used to analyze the fault character firstly. The experiment system of a bearing test rig is shown in Fig. 9. The type of the bearing is 6205-2RS JEM SKF and the sampling frequency is 12 kHz. The structure sizes of rolling bearing are shown in Table 1. The characteristic frequencies of the bearing element faults are shown in Table 2. When the bearing speed is 1797 rpm (1797 / 60 Hz), the fault characteristic frequencies of the inner ring, outer ring and rolling element are shown in Table 3.

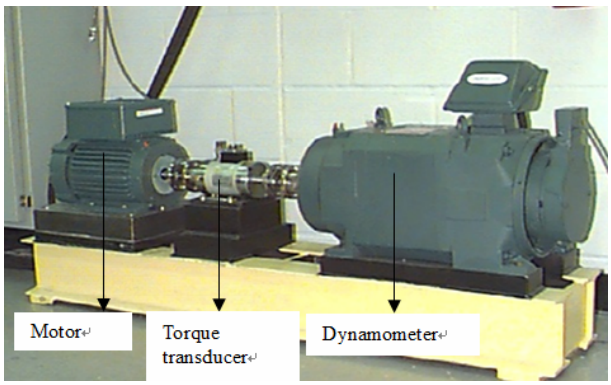

Fig. 9. The experiment system of the bearing test rig.

From Table 3, the defect frequency of the inner ring is 162.19 Hz and calculates its second frequency is 324.38 Hz.

To deal with the experimental signals, the EMD combined

Table 1. The structure size of rolling bearing.

Outside diameter	Inside diameter	Rolling element diameter	Thickness	Pitch diameter	Contact angle	No. of rolling elements
2.0472 inches	0.9843 inches	0.3126 inches	0.5906 inches	1.537 inches	0°	9

Table 2. The defect frequencies of rolling bearing (f_r is running speed in Hz).

Bearing's components	Inner ring	Outer ring	Rolling element
Defect frequencies /Hz	5.4152f_r	3.5848 f_r	4.7135 f_r

Table 3. The defect frequencies with the running speed of 1797 rpm.

Bearing's components	Inner ring	Outer ring	Rolling element
Defect frequencies /Hz	162.19 Hz	107.36 Hz	141.17 Hz

the PSR is used. At the same time, the method of EMD combined with BSR is also used as a comparison. With the development of failure in rolling bearing, some characteristics of deterioration will appear in the vibration signal. A common phenomenon is that the harmonic components of defect frequency will present. Therefore it is a more obvious feature to show the bearing failure in the developing stage. The parameters are set as N = 120000, f_s = 12000 and then resolution is 12000/120000 = 0.1. For the scale transformation method, the rescaling factor m is set as 2000. Then the frequency rescaled is 162.19/ 2000 = 0.081 << 1. In the calculation of SNR, M is set as 160 to estimate the noise intensity around the frequency.

When D = 1.3, the defect frequency is not obvious in the strong noise background. Through the method in this paper, the defect frequency is clearly revealed. Figs. 10 and 11 show the frequency spectrums of the optimal decomposition results at the defect frequency by EMD combined with BSR and EMD combined with PSR, respectively. In Fig. 10, the highest point is located at 161.7 Hz both in IMF5 and IMF6. Because the same frequency is presented in different IMFs, it is another kind of mode mixing phenomena.

In the frequency spectrum at Fig. 11, the highest point is located at 161.7 Hz in IMF6. The defect frequency of inner ring is 162.19 Hz from Table. 3. Without considering the effect of the load, the change in the contact angle of the rolling bearing can lead to a change in the frequency of the failure shock. As a result, there is a deviation between the theoretical defect frequency and the actual defect frequency. This figure doesn't appear the mode mixing problem like Fig. 10.

To explain the phenomenon further, we give Fig. 12 which is related to Figs. 10 and 11. Fig. 12 shows the time domain waveforms and frequency spectrums of BSR and PSR at the defect frequency, respectively. Moreover, the output in Fig. 12 is obtained after adaptive SR but before the procedure of EMD. We use Fig. 12 to explain the reason of mode mixing in

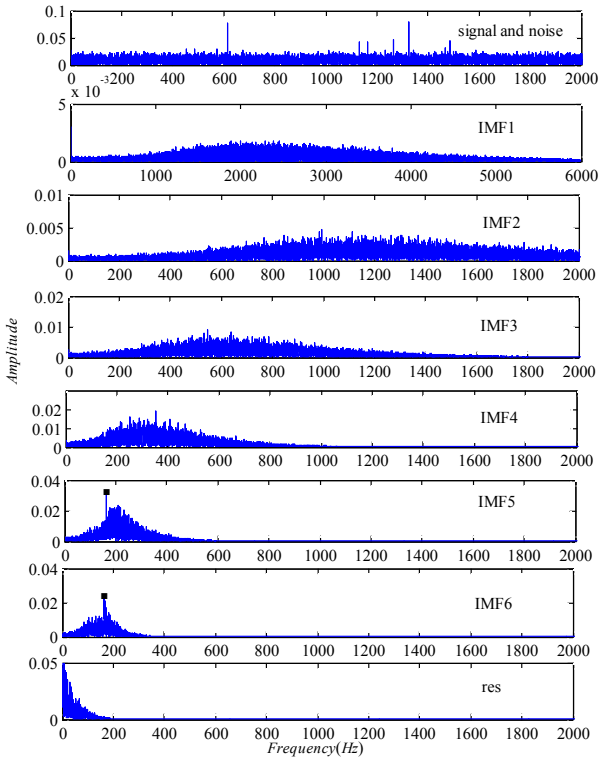

Fig. 10. The frequency spectrum of EMD by BSR at the defect frequency: Optimal output with a = 463.7 and b = 413.736. In IMF5 and IMF6, the highest point is located at 161.7 Hz.

detail. Huang pointed out that the main reason of the mode mixing is intermittence of the signal [42]. Besides the intermittent signal, impulse interference and noise also lead to the mode mixing problem. We call these circumstances anomalous events. Anomalous events will result in the anomalous distribution of local extreme points and then envelope distortion will generate because the smoothness and flexibility of the envelope should be guaranteed. Firstly, we make a comparison of the first subgraph and the third subgraph in Fig. 12. The local extreme points of the time domain waveform of BSR change drastically whereas the time domain waveform of PSR with no similar phenomenon. Therefore, the drastic change of local extreme points is the root cause of the mode mixing problem. Secondly, the second subgraph and the fourth subgraph have some differences. In the frequency spectrum of BSR, we clearly find some noise jamming before the defect frequency. However, there is basically a smooth line which closes to zero before the defect frequency in the frequency spectrum of PSR. The reason of this deference is that the BSR is optimized by two parameters, while the PSR is equivalent to optimizing the infinitely parameters because the

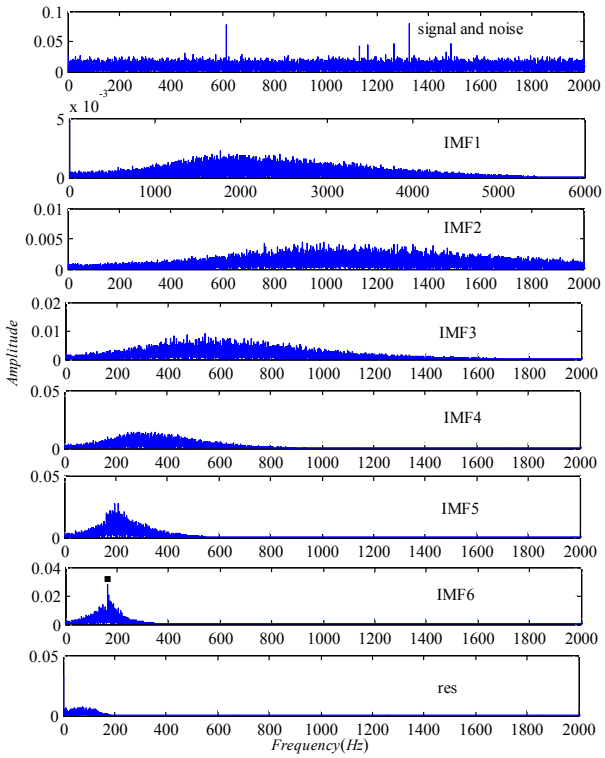

Fig. 11. The frequency spectrum of EMD by PSR at the defect frequency: Optimal output with a = 3148.244 and b = 0.019. In IMF6, the highest point is located at 161.7 Hz.

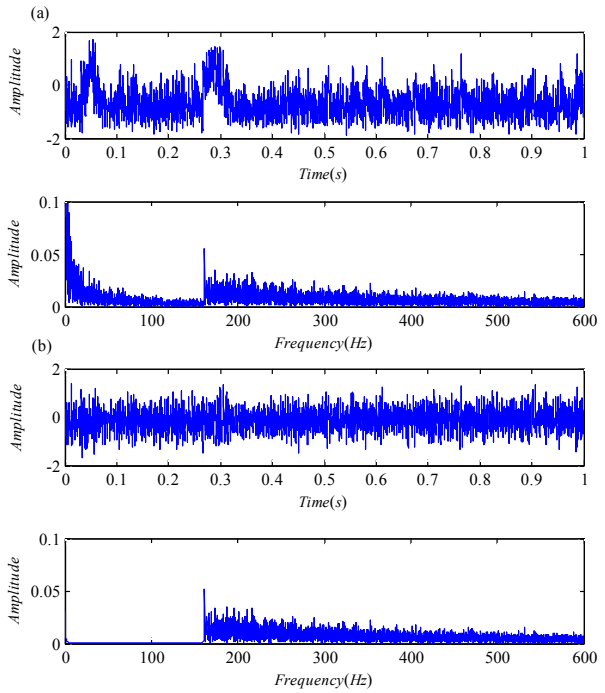

Fig. 12. The time domain waveforms and frequency spectrums of adaptive SR at the defect frequency: (a) The time domain waveform and frequency spectrum of BSR at the defect frequency; (b) the time domain waveform and frequency spectrum of PSR at the defect frequency.

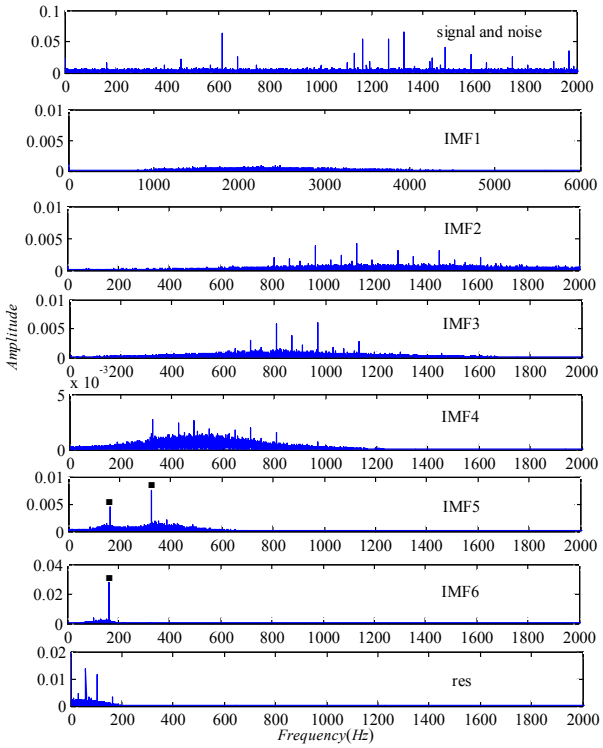

Fig. 13. The frequency spectrum of EMD by BSR at the second harmonic frequency: Optimal output with a = 3.62 and b = 2922.228. In IMF5, the highest points are located at 161.7 Hz and 323.4 Hz, respectively. In IMF6, the highest point is located at 161.7 Hz.

sinx in the equation of PSR will contain infinitely items when it expands into the Maclaurin series. So the effect of the frequency spectrum of PSR is better. As a result, much more noise jamming in the second subgraph will also bring about mode mixing.

When D = 0.1, Figs. 13 and 14 show the frequency spectrums of the optimal decomposition results at its second harmonic frequency by EMD combined with BSR and EMD combined with PSR, respectively. In addition, the signal is preprocessed by a band-stop filter for the purpose of a better effect. In Fig. 13, the highest points are located at 161.7 Hz and 323.4 Hz in IMF5. In IMF6, the highest point is located at 161.7 Hz. 323.4 Hz is twice the actual defect frequency 161.7 Hz and instead of theoretical second harmonic frequency 324.38 Hz. As we mentioned before that different frequencies appear in the same IMF, it is also reveals mode mixing phenomena.

In Fig. 14, the highest point is located at 323.4 Hz in IMF4 and 161.7 Hz is the highest point in IMF5. This figure shows the successful decomposition because 161.7 Hz and 323.4 Hz has clearly appeared in different IMFs.

Compared with Figs. 10 and 11, Figs. 13 and 14, we obtain the conclusion that the method of EMD combined with PSR is much better than the method of EMD combined with BSR.

In order to further verify the common of the conclusion, we use the bearing failure data collecting in our laboratory to

Table 4. The structure size of rolling bearing.

Outside diameter	Inside diameter	Rolling element diameter	Thickness	Pitch diameter	Contact angle	No. of rolling elements
2.8346 inches	1.1811 inches	0.3937 inches	0.748 inches	2.047 inches	0°	11

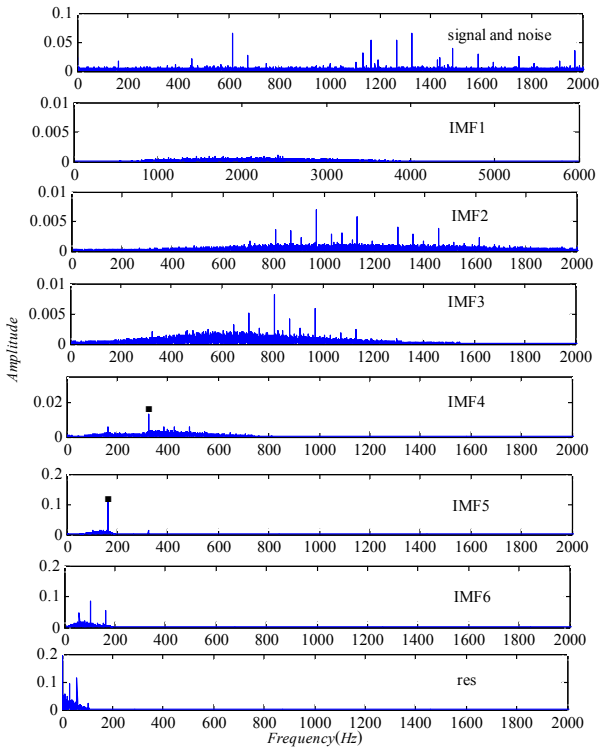

Fig. 14. The frequency spectrum of EMD by PSR at the second harmonic frequency: Optimal output with a = 3941.9 and b = 0.39. In IMF4, the highest point is located at 323.4 Hz. In IMF5, the highest point is located at 161.7 Hz.

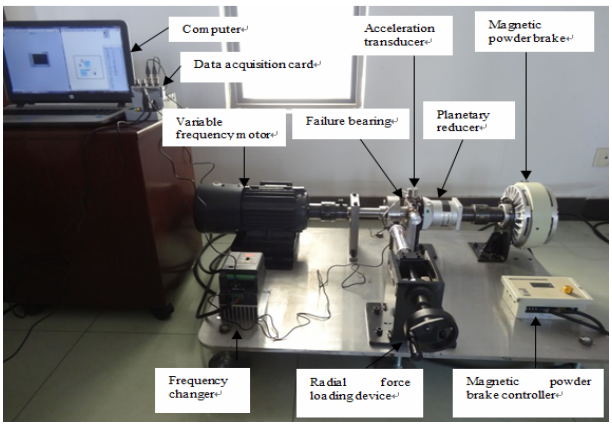

Fig. 15. The experiment system of the bearing test rig.

support it. The experimental system of a bearing test rig is shown in Fig. 15. This fault diagnosis of the bearing is based on the scratch fault. The type of the bearing is N306E and the structure sizes of rolling bearing are shown in Table 4. When collecting the experimental signal, a piezoelectric acceleration

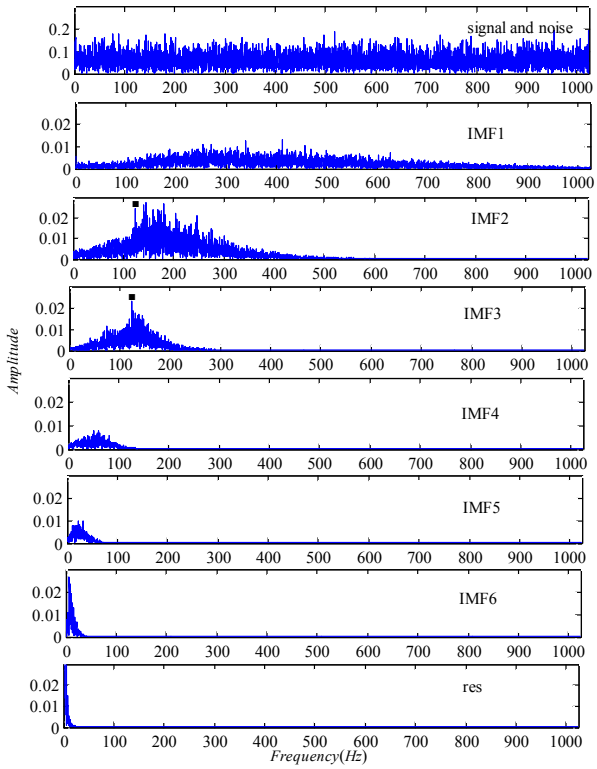

Fig. 16. The frequency spectrum of EMD by BSR at the defect frequency: Optimal output with a = 675.47 and b = 1708.97. In IMF2, one of the highest points is located at 124 Hz. In IMF3, the highest point is located at 124 Hz.

sensor is used and sampling frequency is 2048 Hz. When the bearing speed is 1494 rpm (1494 / 60 Hz), we can calculate the theoretical fault frequency of bearing rolling element is 124.69 Hz and its theoretical second frequency is 249.38 Hz. The parameters are set as N = 10240, f_s = 2048, M = 160 and then the resolution is 2048/10240 = 0.2.

In order to simulate the actual situation, D is set as 6 to make fault information submerged in the noise. m is set as 2000 and then the frequency rescaled is 124.69/ 2000 = 0.0623 << 1, Figs. 16 and 17 show the frequency spectrums of the optimal decomposition results at its defect frequency by EMD combined with BSR and EMD combined with PSR, respectively. In Fig. 16, 124 Hz appears both in IMF2 and IMF3. As mentioned above, it is a mode mixing problem.

In the frequency spectrum at Fig. 17, the highest point is located at 124 Hz in IMF3. The mode mixing phenomenon does not appear as it in Fig. 16.

When D = 1, the second harmonic frequency is not obvious. M is as 3000 and then the frequency rescaled is 249.38/3000 =

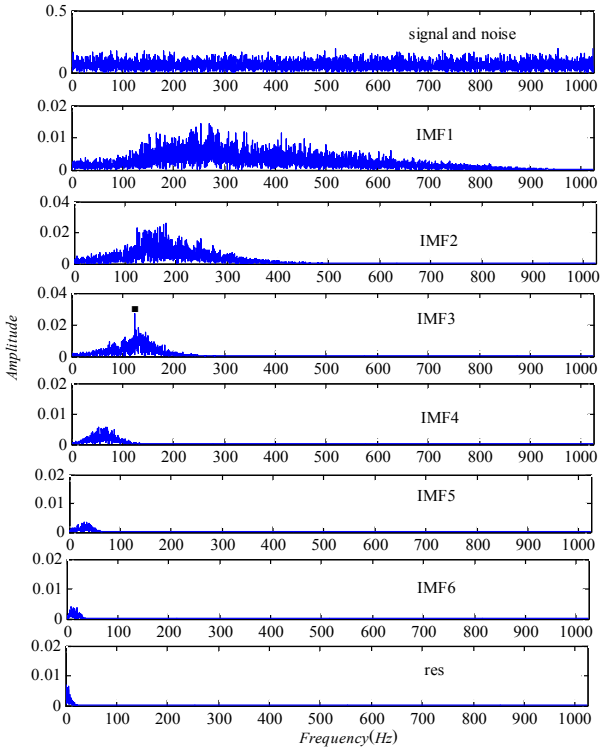

Fig. 17. The frequency spectrum of EMD by PSR at the defect frequency: Optimal output with a = 1778.291 and b = 0.19987. In IMF3, the highest point is located at 124 Hz.

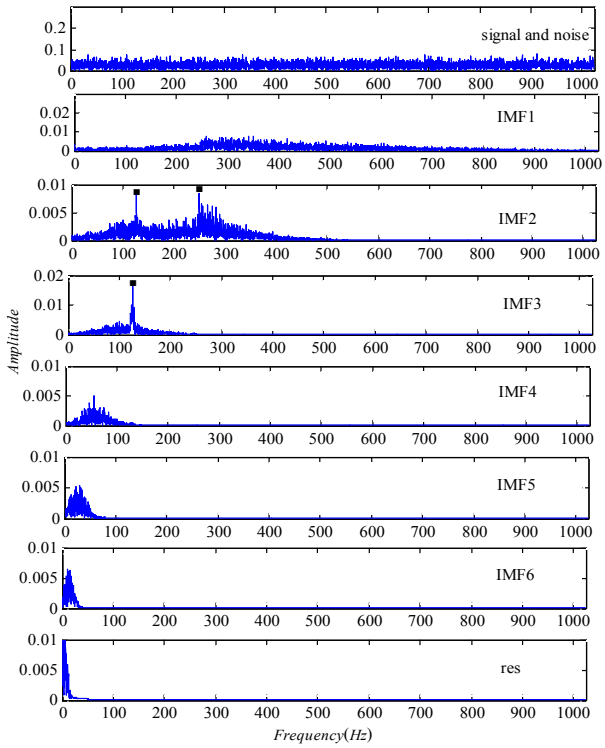

Fig. 18. The frequency spectrum of EMD by BSR at the second harmonic frequency: Optimal output with a = 1306.62 and b = 11314.6. In IMF2, the highest points are located at 125.4 Hz and 248.6 Hz. In IMF3, the highest point is located at 125.4 Hz.

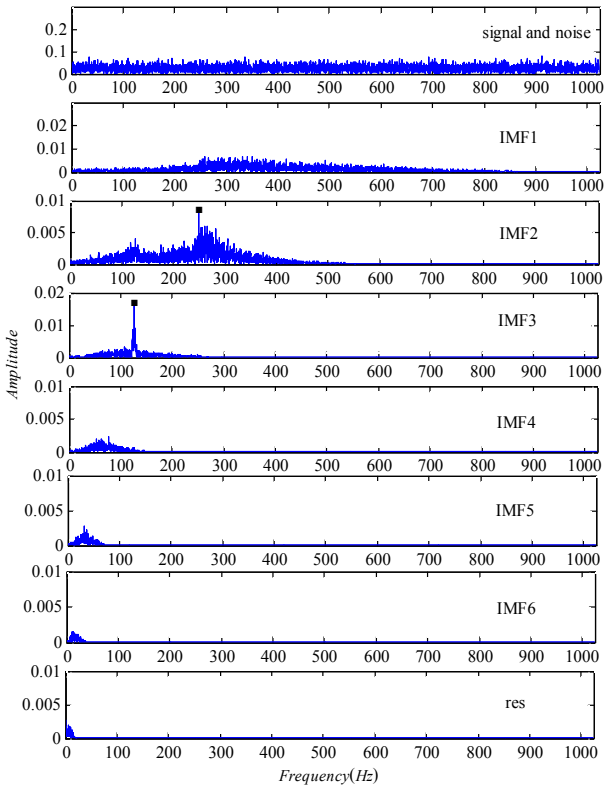

Fig. 19. The frequency spectrum of EMD by PSR at the second harmonic frequency: Optimal output with a = 124.288 and b = 6.782. In IMF2, the highest points are located at 248.6 Hz. In IMF3, the highest point is located at 125.4 Hz.

0.083 << 1. Moreover, the signal is preprocessed by band-stop filter to remove useless waves. Figs. 18 and 19 show the frequency spectrums of the optimal decomposition results at second harmonic frequency by EMD combined with BSR and EMD combined with PSR, respectively.

In IMF2 in Fig. 18, the highest points are located at 125.4 Hz and 248.6 Hz. In IMF3, the highest point is located at 125.4 Hz. It also shows a mode mixing problem.

In Fig. 19, 248.6 Hz and 125.4 Hz appear in IM2 and IMF3, respectively. This figure illustrates the method of EMD combined with PSR is an effective method.

Compared with Figs. 16 and 17, Figs. 18 and 19, we find that the EMD combined with the PSR can deal with the experimental signals much more excellently than EMD combined with the BSR.

By analyzing these two series of experimental data, the effectiveness of the EMD combined with the PSR in decomposing the multi-frequency signal is verified.

6. Conclusions

In this paper, we propose a method of EMD combined with the adaptive SR to deal with the multi-frequency signal submerged into noisy background. The original signal cannot be decomposed by the EMD only. We realize the decomposition

by EMD combined with the PSR. The main highlights and conclusions are as following:

(1) A general scale transformation is proposed and the random particle swarm optimization is used to realize the adaptive SR.

(2) The signal cannot be decomposed by the EMD combined with the traditional BSR. However, it can be decomposed successfully by the EMD combined with the PSR which is proposed in this paper. In other words, the method of EMD combined with PSR is superior to EMD combined with BSR.

(3) This method can not only deal with the simulation signal successfully, but also analyze the experimental signal excellently. Therefore, it can be used in the bearing fault diagnosis.

Although the method proposed in this paper has its advantages, some other problems still exist. For example, the noise in our study is considered as a white noise. However, in the real industrial engineering, the noise is not a white noise but a real one, such as the Poisson noise, the colored noise, the non-Gaussian noise, the bounded noise, etc. Under these complex and real noisy background, whether the method in this paper can be still used in decomposing the multi-frequency signal is an open problem. We will do our best to study this problem further. Especially, we will focus on the method of EMD combined with SR in the complex and real noisy background in our future work.

Acknowledgment

We acknowledge financial supports by the National Natural Science Foundation of China (Grant No 11672325), the Fundamental Research Funds for the Central Universities (Grant No 2015XKMS023), Top-notch Academic Programs Project of Jiangsu Higher Education Institutions and the Priority Academic Program Development of Jiangsu Higher Education Institutions.

Nomenclature

t	: Time
A	: Amplitude
D	: Noise intensity
f	: Frequency
ω_j	: Angular frequency
$U(x)$	: Potential function

References

[1] Huang et al., The empirical mode decomposition and the Hilbert spectrum for nonlinear and non-stationary time series analysis, *Proc. R. Soc. Lond. A,* 454 (1998) 903-995.

[2] Y. F. Yang and Y. F. Wu, *Applications of Empirical Mode Decomposition in Vibration Analysis*, First Ed., National Defence Industry Press, Beijing, China (2013).

[3] Xiong et al., Low-speed rolling bearing fault diagnosis based on EMD denoising and parameter estimate with alpha stable distribution, *J. Mech. Sci. Technol.,* 31 (4) (2017) 1587-1601.

[4] Lei et al., A review on empirical mode decomposition in fault diagnosis, *Mech. Syst. Signal. Pr.,* 35 (2013) 108-126.

[5] S. Singh and N. Kumar, Combined rotor fault diagnosis in rotating machinery using empirical mode decomposition, *J. Mech. Sci. Technol*., 28 (12) (2014) 4869-4876.

[6] Dong et al., Sifting process of EMD and its application in rolling element bearing fault diagnosis, *J. Mech. Sci. Technol.,* 23 (8) (2009) 2000-2007.

[7] Y. Lv, R. Yuan and G. B. Song, Multivariate empirical mode decomposition and its application to fault diagnosis of rolling bearing, *Mech. Syst. Signal. Pr.,* 81 (15) (2016) 219-234.

[8] Li et al, An improvement EMD method based on the optimized rational Hermite interpolation approach and its application to gear fault diagnosis, *Measurement*, 63 (2015) 330-345.

[9] D. J. Yu, J. S. Cheng and Y. Yang, Application of EMD method and Hilbert spectrum to the fault diagnosis of roller bearings, *Mech. Syst. Signal. Pr.,* 19 (2) (2005) 259-270.

[10] X. F. Liu, L. Bo and H. L. Luo, Bearing faults diagnostics based on hybrid LS-SVM and EMD method, *Measurement*, 59 (2015) 145-166.

[11] J. Cheng, D. Yu and Y. Yang, The application of energy operator demodulation approach based on EMD in machinery fault diagnosis, *Mech. Syst. Signal. Pr.,* 21 (2) (2007) 668-677.

[12] J. S. Cheng, D. J. Yu and Y. Yang, A fault diagnosis approach for roller bearings based on EMD method and AR model, *Mech. Syst. Signal. Pr.,* 20 (2) (2006) 350-362.

[13] Shi et al., Signal feature extraction based on cascaded multi-stable stochastic resonance denoising and EMD method, *Measurement*, 90 (2016) 318-328.

[14] Chen et al., Research of weak fault feature information extraction of planetary gear based on ensemble empirical mode decomposition and adaptive stochastic resonance, *Measurement*, 73 (2015) 55-67.

[15] Zhang et al., Enhanced detection of rolling element bearing fault based on stochastic resonance, *Chin. J. Mech. Eng*., 25 (6) (2012) 1287-1297.

[16] B. C. Zhou and W. Xu, Stochastic resonance in an asymmetric bistable system driven by mixed periodic force and noises, *Acta . Phys. Sin.,* 56 (10) (2007) 5623-5628.

[17] F. Long, W. Guo and D. C. Mei, Stochastic resonance induced by bounded noise and periodic signal in an asymmetric bistable system, *Physica A,* 391 (22) (2012) 5305-5310.

[18] Gammaitoni et al., Stochastic resonance, *Rev. Mod. Phys.,* 70 (1) (1998) 223.

[19] M. J. Zhang, J. Tang and X. H. He, *EEMD method and its application in mechanical fault diagnosis*, First Ed., National Defence Industry Press, Beijing (2015).

[20] Xu et al., Stochastic resonance with tuning system parameters: the application of bistable systems in signal processing, *Chaos. Solitons. Frac.,* 13 (4) (2002) 633-644.

[21] Lei et al., Planetary gearbox fault diagnosis using an adaptive stochastic resonance method, *Mech. Syst. Signal. Pr.,* 38 (1)

(2013) 113-124.
[22] Z. Y. Lu, T. Y. Yang and M. Zhu, Study of the method of multi-frequency signal detection based on the adaptive stochastic resonance, *Abstr. Appl. Anal.,* 2 (2013) 360-374.
[23] Zhou et al., Novel synthetic index-based adaptive stochastic resonance method and its application in bearing fault diagnosis, *J. Sound. Vib.,* 391 (2017) 194-210.
[24] Tan et al., Study of frequency-shifted and re-scaling stochastic resonance and its application to fault diagnosis, *Mech. Syst. Signal. Pr.,* 23 (3) (2009) 811-822.
[25] Leng et al., Engineering signal processing based on bistable stochastic resonance, *Mech. Syst. Signal. Pr.,* 21 (1) (2007) 138-150.
[26] D. Dai and Q. He, Multiscale noise tuning stochastic resonance enhances weak signal detection in a circuitry system, *Meas. Sci. Technol.,* 23 (11) (2012) 115001.
[27] Q. He and J. Wang, Effects of multiscale noise tuning on stochastic resonance for weak signal detection, *Digit. Signal. Process.,* 22 (4) (2012) 614-621.
[28] Gammaitoni et al., Stochastic resonance, *Rev. Mod. Phys.,* 70 (1998) 223-287.
[29] B. Mcnamara and K. Wiesenfeld, Theory of stochastic resonance, *Phys. Rev. A,* 39 (1989) 4854-4869.
[30] C. Nicolis, Stochastic resonance in multistable systems: The role of intermediate states, *Phys. Rev. E,* 82 (2010) 011139.
[31] S. Saikia, The role of damping on stochastic resonance in a periodic potential, *Phys. A,* 416 (2014) 411-420.
[32] K. H. Liu and Y. F. Jin, Stochastic resonance in periodic potentials driven by colored noise, *Phys. A,* 392 (2013) 5283-5288.
[33] J. H. Yang and X. B. Liu, Sequential vibrational resonance in multistable systems, *arXiv preprint arXiv: 1106.3431* (2011).
[34] Liu et al., Improving the bearing fault diagnosis efficiency by the adaptive stochastic resonance in a new nonlinear system, *Mech. Syst. Signal. Pr.,* 96 (2017) 58-76.
[35] Lu et al., Enhanced rotating machine fault diagnosis based on Time-delayed feedback stochastic resonance, *J. Vib. Acoust.,* 137 (2015) 051008.
[36] Chen et al., Research of weak fault feature information extraction of planetary gear based on ensemble empirical mode decomposition and adaptive stochastic resonance, *Measurement*, 73 (2015) 55-67.
[37] F. Marini and B. Walczak, Particle swarm optimization (PSO). A tutorial, *Chemometr. Intell. Lab.,* 149 (2015) 153-165.
[38] N. B. Guedria, Improved accelerated PSO algorithm for mechanical engineering optimization problems, *Appl. Soft. Comput.,* 40 (2016) 455-467.
[39] I. G. Tsoulos and A. Stavrakoudis, Enhancing PSO methods for global optimization, *Appl. Math. Comput.,* 216 (2010) 2988-3001.
[40] A. Ichiki and Y. Tadokoro, Signal-to-noise ratio improvement by stochastic resonance in moments in non-dynamical systems with multiple states, *Phys. Let. A,* 377 (2013) 185-188.
[41] *http://csegroups.case.edu/bearingdatacenter/pages/download-data-file.*
[42] N. E. Huang et al., A new view of nonlinear waves: The Hilbert spectrum, *Annu. Rev. Fluid. Mech.,* 31 (1999) 417-457.

Jingling Zhang received her B.Sc. degree in 2016 from Jiangsu Normal University, Jiangsu, China. Now she is a master degree candidate in China University of Ming and Technology. Her main research interest is equipment fault diagnosis.

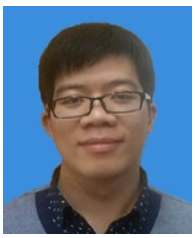

Dawen Huang received his B.Sc. degree in 2016 from Heibei University of Engineering, Heibei, China. Now he is a master degree candidate in China University of Ming and Technology. His main research interest is equipment fault diagnosis.

Jianhua Yang received the Ph.D. degree in State Key Laboratory of Mechanics and Control of Mechanical Structures from Nanjing University of Aeronautics and Astronautics, Nanjing, China, in 2011. Now he is an Associate Professor in China University of Mining and Technology. His main research interest includes equipment fault diagnosis, intelligent maintenance system, nonlinear vibration, and novel engineering machineries.

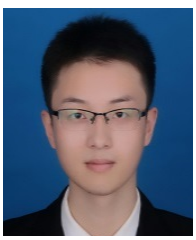

Xiaole Liu received his B.Sc. degree and is a master degree candidate in China University of Ming and Technology. His main research interest is equipment fault diagnosis.

Houguang Liu received the Ph.D. degree in State Key Laboratory of Mechanical System and Vibration from Shanghai Jiao Tong University, Shanghai, China, in 2011. Now he is an Associate Professor in China University of Mining and Technology. His current research interests include mechanical vibration analysis and control, vibration signal processing, and fault diagnosis.